

## PHYSICAL PROPERTIES OF NANOSTRUCTURED ZnO THIN FILMS DEPOSITED BY DC MAGNETRON SPUTTERING METHOD WITH DIFFERENT VOLUME OF O<sub>2</sub> IN A CARRIER GAS

S. Asgary <sup>\*a</sup>, A.H. Ramezani <sup>a</sup>, A. Mahmoodi <sup>b</sup>

<sup>a\*</sup> Department of Physics, West Tehran Branch, Islamic Azad University, Tehran, Iran

<sup>b</sup> Plasma physics Research Center, Science and Research Branch, Islamic Azad University, Tehran, Iran

(Received 12 April 2018; accepted 21 January 2019)

### Abstract

High-quality ZnO thin films with polycrystalline hexagonal structure and (101) preferentially oriented were deposited on Si and corning glass substrates by reactive direct current magnetron sputtering. The effects of different oxygen concentration in carrier gas on structural, morphological and optical properties have been investigated. The increase of O<sub>2</sub> concentration resulted in the decrease of preferred orientation intensity and peak shifting to lower 2θ values. Scanning electron microscopic images showed a porous tapered columnar structure similar to the zone I of Thornton's structure zone model at lower O<sub>2</sub> content and a smooth microstructure similar to the zone T structure at highest O<sub>2</sub> content. AFM images showed that film morphology and surface roughness were influenced by O<sub>2</sub> concentration. UV-Vis-NIR measurements indicated that the UV absorption intensity of samples was increased and shifted to shorter wavelength (blue shift) at higher O<sub>2</sub> concentration. Moreover, the optical band gap increased from 3.91 to 4.41 eV as a function of the oxygen concentration.

**Keywords:** DC magnetron sputtering; Porous ZnO thin film; Structural properties; Morphological properties; Optical band gap; Absorbance

### 1. Introduction

ZnO is a II-VI binary compound semiconductor that exhibits unique features like excellent physical, chemical and bio-compatible properties [1], and it is extensively used in wide range of applications. ZnO has more advantages over III-nitride semiconductors, such as availability of high-quality bulk substrates, higher exciton binding energy and ease of wet etching [2].

It crystallizes in three forms, such as wurtzite, zinc blend and rock salt. But hexagonal wurtzite phase of ZnO is thermodynamically more stable than other phases, especially at room temperature [3]. ZnO has a wide and direct band gap of 3.37 eV with large exciton binding energy of 60 meV [4]. Its especial physical properties, such as high electron mobility, high thermal conductivity, high transparency in visible wavelength, strong room temperature luminescence, high electron mobility and high piezoelectric coefficients [5] make ZnO a good candidate for photonic applications in the UV and

blue spectral range, opto-electronic devices [6], solar cells devices [7], light-emitting diodes, liquid crystal displays, anti-reflective coatings, electrochromic displays, gas sensors and spintronic applications [8]. In addition, ZnO has extensive applications in manufacturing, pharmaceutical and health-care products, bactericidal activity, UV protection, ceramics, cement, cosmetics, lubricants, glass, paints and coatings [9].

Recent advancement in research on colloidal ZnO nanoparticles and nanostructured ZnO-based biomaterials has initiated their use in biomedical application, such as in targeted drug delivery, bioimaging and biosensing [10].

Other applications of ZnO films are for optical waveguides [11], transparent conducting coatings [12] acoustic wave transducer [13], acousto-optic and acousto-electronic devices [14].

Pure ZnO is unstable and it becomes resistive due to the presence of oxygen vacancies or point defects. Generally, ZnO at room temperature exhibits n-type electrical conductivity because of Zn interstices and

\*Corresponding author: sima198124@yahoo.com



oxygen vacancies [15]. It can be purposely doped to become p-type using group-I elements such as Li, Na and Ag or group V elements such as N, P and As.

ZnO has different nano-shapes which include nanorod [16], nanowire [17], nanotube [18] hollow nanospheres [19], and colloidal nanoparticles [20].

ZnO thin films, nanotubes and nanowires are thermodynamically stable and their properties can be easily tailored by altering its synthesis route, dimensions and surface to volume ratio [21].

There are different methods to prepare nanostructured thin ZnO films such as DC sputtering, molecular beam epitaxy, vacuum evaporation, chemical vapor deposition, sol-gel processing, RF magnetron sputtering [22], spray pyrolysis, pulsed laser deposition (PLD), chemical spray [23] and plasma enhanced chemical vapor deposition [24].

Among physical methods, sputtering represents a special class of depositing technique due to its high deposition rate, high adhesion to the substrate, low substrate temperature, good adhesion of films on substrates, and it is compatible with engineering at the industrial scale as well [25]. Direct current (DC) magnetron sputtering could be a potential technique for synthesizing thin films, nanostructured coatings and various metal nanoparticles, including metallic oxide, nitride and carbide films [26-28]. DC magnetron sputtering is widely used in the semiconductor technology manufacturing, because of producing high quality ZnO films with controlled stoichiometry of the films, thickness and morphology [29].

The thin films that are obtained by sputtering technique have generally polycrystalline structure [30].

The structural and optical properties of films obtained by DC cylindrical magnetron sputtering setup, with different oxygen volume in reactive gas have been investigated extensively. The  $O_2$  amounts in plasma play a key role in the synthesis of nanostructured ZnO thin films. The preferred orientation, grain size, morphology, optical absorbance and band gap energy of the thin films are influenced by argon/oxygen concentration in the reactive gas. In this paper, the nano thin films with different grain size were provided. Size evolutions of semiconducting nanoparticles have become essential for exploring the properties of the material.

The estimated band gaps ( $E_g$ ) of the ZnO layers were determined using Tauc equation as a function of the oxygen ratio.

## 2. Experimental

The DC magnetron sputtering setup consisted of two coaxial cylinders, the inner cylinder as target (cathode), and the outer cylinder as a sample keeper

(anode), which is shown in Fig. 1. The zinc metallic target with 99.99% purity, 1.5 cm radius and 20 cm height was used as a target. The substrates were cleaned with deionized water, acetone and ethanol under ultrasonic vibrations for 15 minutes. In order to eliminate surface contamination of the target, the pre-sputtering was carried out for 10 minutes. The cleaned substrates were fixed inside the outer cylinder. The deposition chamber was cleaned to  $2 \times 10^{-5}$  Torr to remove residual gases present in the chamber with Alcatel ACT-600 rotary pump and diffusion pumps, respectively. An Ar +  $O_2$  gas flow controlled by a mass flow controller was admitted into the chamber. Different volumes of  $O_2$  + Ar gas mixtures ((95% Ar+5%  $O_2$ ), (90%Ar + 10%  $O_2$ ) and (85%  $O_2$  +15%  $O_2$ )) were used as carrier gas in the experiment.

The other sputtering parameters, such as working pressure and sputtering power, were  $2 \times 10^{-2}$  Torr and 210 W, respectively, and they were kept constant during the deposition process. The magnetron current was 0.35 A, which required a discharge voltage of 600 V, independent on the gas mixture. The time for deposition was 5 min.

The films structures were investigated by a STOE SIADI MP X-ray diffractometer using Cu K $\alpha$  ( $\lambda = 0.15405$  nm) radiation, tungsten filament at 40 kV, 40 mA and step size of  $0.04^\circ$  with ( $\theta$ - $2\theta$ ) geometry. The field emission scanning electron microscopy (FE-SEM; Hitachi, S-4800) at 5 kV and 20  $\mu$ A was carried out to analyze the films morphology. An atomic force microscopy (AFM) system (Park systems XE-100) with non-contact mode was used for the investigation of surface morphology. The optical absorbance spectra were collected by a Cary 500 UV-vis-NIR Spectrophotometer with a wavelength range of 300-1500 nm.

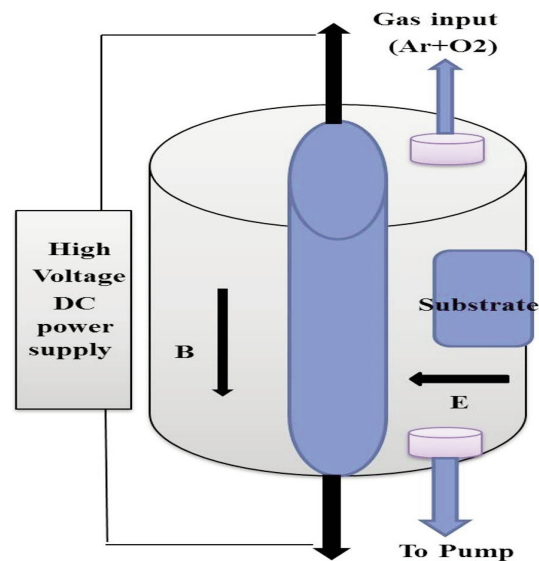


Figure 1. Schematic diagram of sputtering setup

### 3. Results and discussion

#### 3.1 XRD

The XRD method was used for analyzing the structure parameters such as crystallite size, microstrain and dislocation density. The crystallographic structure of the materials is shown in Fig.2.

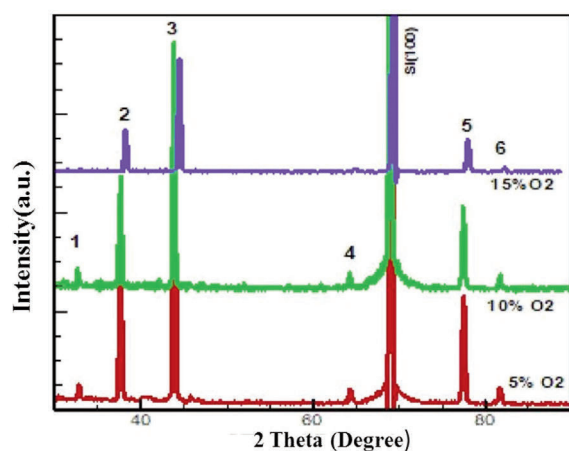


Figure 2. XRD patterns of the ZnO thin films at different O<sub>2</sub>% in plasma deposited on Si substrates

The XRD spectrum clearly shows the crystalline structure of the nanoparticles and various peaks of zinc oxide. All the samples are well crystallized in ZnO hexagonal wurtzite structures (JCPDS 36-1451), except for the peak located at 43.77°, which is associated with the (101) crystal plane of hexagonal Zn. The multi structure of nanoparticles shows that the peaks intensity has changed for different samples.

Tables 1-3 show the XRD information of the three samples.

At O<sub>2</sub>=5 and 10 %, the samples showed polycrystalline nature by the appearance of several peaks at 2θ=32.65°, 37.53°, 64.19°, 77.36° and 81.55° corresponds to (100), (101), (103), (202) and (104) crystal plans, respectively. The peak at 69.5° arises from the Si (100) substrate.

The intensity of peaks seems to be effectively affected by O<sub>2</sub> concentration in mixture gas. The XRD spectrum shows a stronger diffraction peaks at O<sub>2</sub>=5%. According to the XRD result, with increasing the O<sub>2</sub>%, the intensity of all zinc and the complex oxides peaks concomitantly decreased, and the (100) and (103) diffraction plans disappeared with increasing O<sub>2</sub> concentration to 15%. Therefore, the O<sub>2</sub> concentration in gas mixture deteriorated the crystallinity of the ZnO films. The optimum growth conditions depend on crystalline quality and surface morphology.

The XRD peak positions of the films changed and slightly shifted towards higher 2θ side at higher O<sub>2</sub>

concentration in gas mixture, which indicates that the lattice parameter decreased with the increase of O<sub>2</sub> concentration (change in d will cause a shift in the diffraction pattern).

According to Bragg's law, if the spacing of the crystallographic planes (d-spacing) changes, the Bragg angle should either decrease or increase. The tensile stress increases the d-spacing which causes a shifting of peak towards lower 2θ values in the XRD pattern whereas compression stress decreases the d-spacing which results in the shifting of peaks towards higher 2θ values.

The XRD analysis identified different details about phase compositions, crystal preferred orientations and crystal defect concentrations [31].

The (101) peak has the highest intensity as preferred orientation. Many scientists analyzed the ZnO thin films with the major orientation (101) along the axis [32]. The accumulated ad-atoms occupy positions with minimum energy by surface diffusion. It means that the preferred orientation is the greatest close-packed plane with the lowest surface energy.

The XRD pattern confirms that at 5% and 10% O<sub>2</sub> in gas mixture, the (100) peak is almost seven orders of magnitude weaker than the (101) peak, indicating the presence of very minor amounts of ZnO grains oriented with the c-axis perpendicular to the plane [33].

The variations in the diffraction peaks can be attributed to the stress built in the films during the nucleation process. The films grown by PVD methods are often stressed (tensile or compressive) because of the formation of non-equilibrium microstructures. Compressive stress is attributed to the energetic particle bombardment in PVD grown films [34]. Although anisotropy in growth is an inherent property of material, deposition rate and top surface of layers can influence the growth rate of ZnO thin film, especially in a particular plane.

Debye-Scherrer's formula was used to calculate the crystallite sizes as given below.

$$D = 0.94\lambda / (\beta \cos\theta) \quad (1)$$

Where D is the crystallite size, λ is the X-ray wavelength, β is the full-width at half the maximum intensity (FWHM) in radians, and θ is the Bragg angle in degrees [35].

The crystallite size of the ZnO thin films increased with increasing O<sub>2</sub> in plasma from 5% to 10%, which may be a result of increasing of imperfections that improve grain boundary mobility and growth rate [36].

The decrease of the crystallite size at 15% O<sub>2</sub> in plasma may be attributed to the increasing of nucleation centers leading to the formation of small grains (from XRD and AFM measurements). The line

**Table 1.** XRD information of ZnO thin film prepared at 5%O<sub>2</sub> in plasma

Peak	2θ /degree	FWHM	d /°A	hkl	Phase
1	32.84	0.23	2.72	(100)	Hexagonal, ZnO
2	37.60	0.39	2.39	(101)	Hexagonal, ZnO
3	43.83	0.39	2.06	(101)	Hexagonal, Zn
4	64.27	0.31	1.44	(103)	Hexagonal, ZnO
5	77.44	0.39	1.23	(202)	Hexagonal, ZnO
6	81.66	0.38	1.17	(104)	Hexagonal, ZnO

**Table 2.** XRD information of ZnO thin film prepared at 10%O<sub>2</sub> in plasma

Peak	2θ /degree	FWHM	d /°A	hkl	Phase
1	32.84	0.23	2.73	(100)	Hexagonal, ZnO
2	37.56	0.27	2.41	(101)	Hexagonal, ZnO
3	43.79	0.39	2.06	(101)	Hexagonal, Zn
4	64.30	0.47	1.44	(103)	Hexagonal, ZnO
5	77.32	0.19	1.23	(202)	Hexagonal, ZnO
6	81.60	0.57	1.17	(104)	Hexagonal, ZnO

**Table 3.** XRD information of ZnO thin film prepared at 15%O<sub>2</sub> in plasma

Peak	2θ / degree	FWHM	d /°A	hkl	Phase
1	38.13	0.43	2.35	(101)	Hexagonal, ZnO
2	44.39	0.47	2.04	(101)	Hexagonal, Zn
3	64.92	0.94	1.43	(103)	Hexagonal, ZnO
4	77.95	0.39	1.22	(202)	Hexagonal, ZnO
5	82.19	0.57	1.17	(104)	Hexagonal, ZnO

broadening that results in small crystallite size in the growth direction of the coating depends on different factors such as strains, dislocations, point defects and stacking faults [37]. The deviation from perfect lattice organization can be obtained by using Stokes Wilson equation [38] as given in Eq. (2)

$$\varepsilon = \beta/4\tan\theta \quad (2)$$

Where 'ε' is internal strain, 'β' is the FWHM of the samples peaks and 'θ' is Bragg's Angle.

Table 4 lists the particle sizes, lattice strain and dislocation density of the preferred (101) plane of ZnO prepared samples.

Real crystal is not perfectly arranged as it has some lattice imperfections, such as stacking faults, dislocation, grain boundaries, etc.

The lattice spacing is equal to the reciprocal of the spatial frequency. The lattice constant can be found from the lattice spacing for a zinc blende material with the x-axis oriented along the [hkl] Miller direction, where the lattice constant is given as

$$a_x = 2d_x \sqrt{h^2 + k^2 + l^2},$$

where  $a_x$  is the lattice constant and  $d_x$  is the lattice spacing in the x-direction. The equation is also valid for the y-direction with appropriate substitutions [39]. The strain greatly depends on the lattice spacing. The lattice spacing, which is used to measure the strain in a material, can also change as a result of O<sub>2</sub> variation. The internal strain increased at 10% O<sub>2</sub> concentration, which can be explained by the increase of lattice imperfection.

The dislocation density (δ) is calculated using Williamson & Smallman relation [40]. The higher grain size 'D' indicate a lower dislocation lines/volume with a better crystallinity.

$$\delta = 1/D^2 \quad (3)$$

Where 'D' is the crystallite size calculated by Debye Scherer's formula. In this formula, dislocations are expected to be isotropically distributed in the crystal and to lie along the grain boundary. The dislocation density for dominant (101) plane decreased firstly and then increased at higher O<sub>2</sub> concentration in plasma.

The minimum crystallite size of (101) plane of ZnO samples, that were prepared at 15% O<sub>2</sub> in plasma, had maximum stress, maximum strain and maximum dislocation density compared to the other samples.

**Table 4.** Crystallite size, lattice strain and dislocation density of (101) plane of ZnO prepared samples

Sample	2θ /degree	hkl	Crystallite size/nm	Lattice strain (10 <sup>-3</sup> )	Dislocation density (10 <sup>-3</sup> )
1	37.60	101	22.0	4.9	2.00
2	37.56	101	32.2	3.3	0.96
3	38.13	101	20.0	5.3	2.50

### 3.2 AFM

The evolution of surface morphology of the ZnO thin films sputter, deposited as a function of O<sub>2</sub> concentration in gas mixture, was characterized by AFM, with a scanning area of 1μm x 1μm as it is shown in Figs.3 (a, b, c). All the films are uniform with a relatively smooth surface. As can be seen in Fig. 2a, at 5% O<sub>2</sub> concentration, the homogeneous surface with small spherical grains and roughness = 1.19 is observed which can be attributed to the polycrystalline nature of the film. At 10% O<sub>2</sub> concentration, surfaces topography indicated a prevailing large grain-like surface morphology, with grains homogeneously distributed. The image shows protuberant grain boundaries that indicate the increase of surface roughness. Optical properties (absorption)



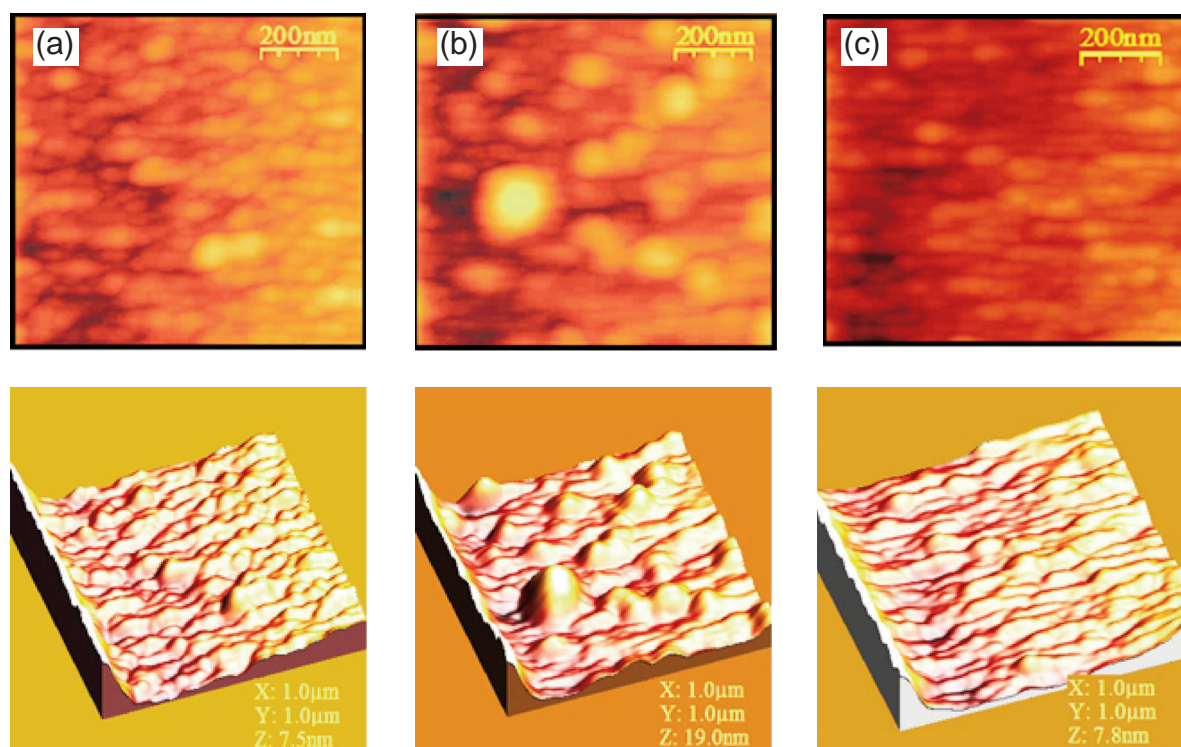


Figure 3. 2D and 3D AFM image of thin films at growth temperature (a) 5%, (b) 10% and (c) 15%  $O_2$  in plasma

strongly depend on grain boundaries. The effect of grain boundaries with inherent space charge regions, due to the interfaces, results in band bending and this is reflected in broadening of the tail end of the absorption in a polycrystalline semiconductor at the band edge [40]. Most of the ZnO nanoparticles, with an average diameter of about 30-40 nm, are spherical. With increasing  $O_2$  concentration in gas mixture from 5% to 10%, an increase in grain size was detected. The increase of the grain size may be attributed to bigger crystallites size and the crystallite agglomeration. Size evolutions of semiconducting nanoparticles become very essential to explore the properties of the material.

At 15%  $O_2$  concentration, the grains oriented

densely, which led to a better surface morphology. The film was composed of particles with an average size estimated to be around 20 nm. It was related to the fact that the highest amounts of oxygen inhibited the growth and coalescence of Zn crystallites by promoting new nucleation centers at the growth front in the presence of oxygen adatoms [41]. These results are in accordance with the XRD data.

The RMS values obtained for  $O_2=10\%$  and 15%  $O_2$  concentration films were found to be around 2.66 nm and 1.18 nm, respectively.

The grain abundance per topography is shown in Fig.4. With increasing  $O_2$  concentration in plasma, the topography did not have remarkable changes, except for  $O_2=10\%$ .

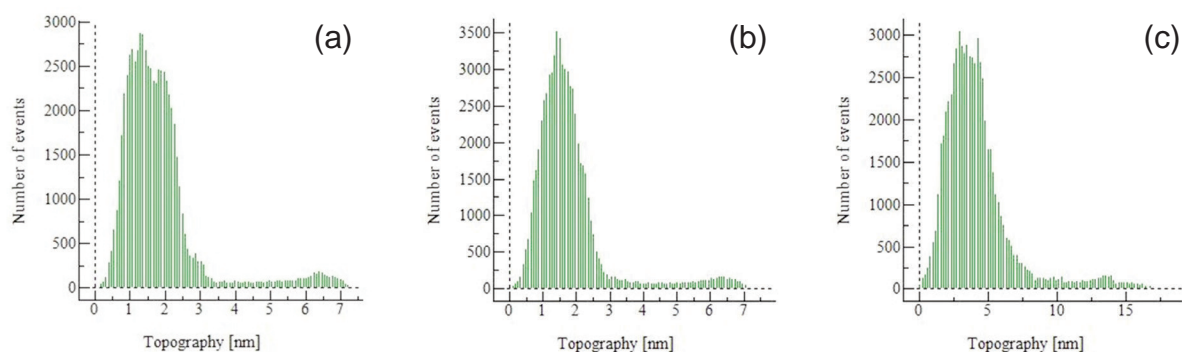


Figure 4. Grain abundance per topography at different  $O_2$  concentration in plasma (a) 5%, (b) 10%, (c) 15%

### 3.3 FESEM

A top-view and cross section of FE-SEM images of ZnO thin films grown at different O<sub>2</sub> % in plasma are presented in Fig.5. The structural and surface morphological properties of the thin films are significantly dependent on the Ar/O<sub>2</sub> ratio in plasma.

At 5% O<sub>2</sub> in plasma, the surface of the ZnO films appears uniform. This case is composed of mixed large needle-like and plate-like crystals with large aspect ratio. The image shows hexagonal rod crystallites with tapered ends similar to the microstructure of zone 1 of Thornton's structure zone model [42]. Because of low adatoms mobility and shadowing effect, the films tend to grow in prefer orientation for minimizing free surface energy, such as c-axis orientation with columnar microstructure.

The growth process at 10% O<sub>2</sub> concentration in plasma has shown a strong change in surface morphology with unique morphology. It appeared as a flower like shape morphology that was composed of mixed tiny granular and lamellar like particles. In these cases, morphology dramatically transformed from plate-like large crystals to a coarse surface structure with grains distributed over the smooth background. It seems that tiny grains combine to form larger nano platelet like structures. Agglomeration of small grains happened due to the grouping of initial nuclei which further caused the formation of a dense

film surface. Irregular plate grains with hundreds of angstrom meter order are randomly distributed with coarseness. This porous structure with large grains was consistent with the XRD results. Increasing the O<sub>2</sub> concentration in plasma resulted in higher density of flakes like features. Change in grain size was due to grouping of little crystallites to form a bigger size.

When the O<sub>2</sub> concentration in the plasma was further increased from 10% to 15%, the ZnO film developed a denser and smoother microstructure similar to the zone T structure. The substrate is fully covered with material. The ZnO nanothin films and their uniform distribution over the substrate, the shape and size of these nanoparticles was confirmed by XRD results.

The thin film exhibits a few small cracks on the surface of the film, suggesting high packing density.

### 3.4 Optical properties

In order to investigate the optical properties and calculate the band gap of ZnO thin films prepared at different O<sub>2</sub> concentration in plasma, the absorbance spectra of the thin films as a function of the wavelength were carried out by UV-vis spectrophotometer was used (Fig.6).

The absorbance was examined by the transmittance (T) and the reflectance (R) spectra by using the following equation:

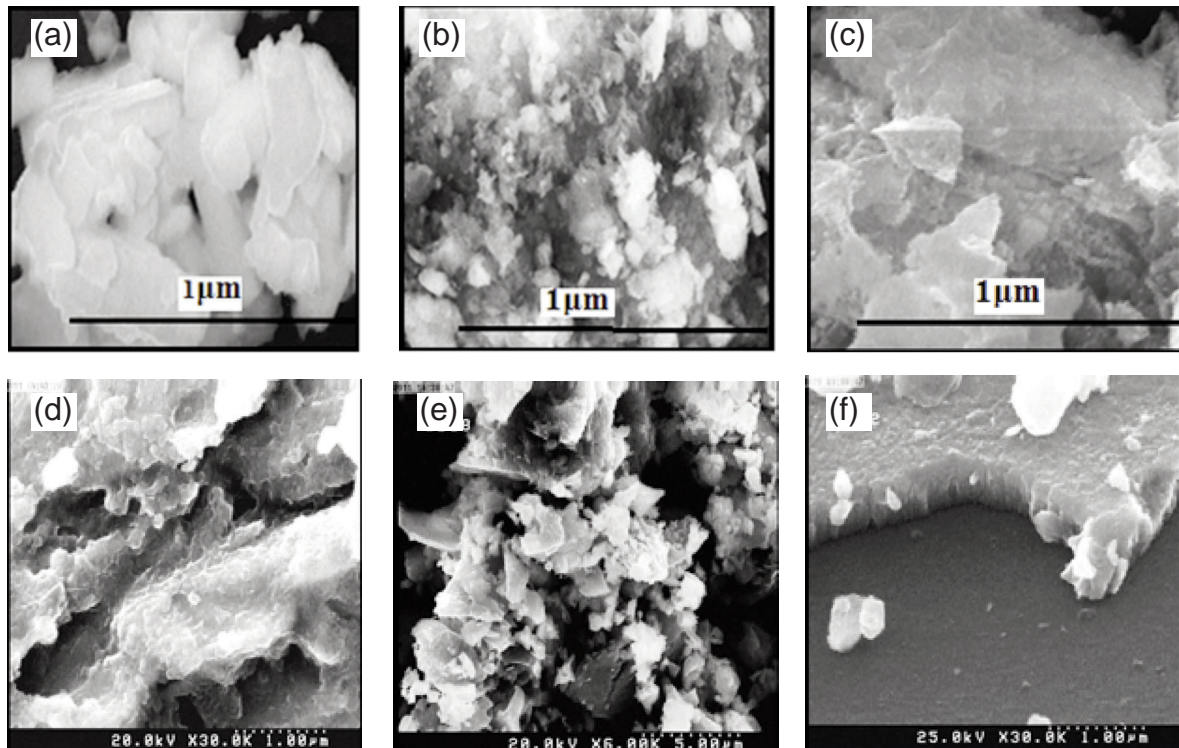


**Figure 5.** The plan view FESEM images of ZnO thin films at (a) 5% O<sub>2</sub>, (b) 10% O<sub>2</sub> and (c) 15% O<sub>2</sub> and cross section images at (d) 5% O<sub>2</sub>, (e) 10% O<sub>2</sub> and (f) 15% O<sub>2</sub> in plasma

$$A\% = 100\% - T\% - R\% \tag{1}$$

All the thin films exhibited the distinctive optical absorption in the UV region of the spectrum. Moreover, the intensity of the absorbance increases with increasing O<sub>2</sub> concentration in carrier gas. The absorption edge relates to the electron transition from valence to conduction band. The 15% O<sub>2</sub> ZnO thin film, exhibited stronger absorption in the UV region compared to the others.

The absorption peak exhibited at 310 nm for 5% O<sub>2</sub> ZnO thin film. For 10% and 15% O<sub>2</sub> ZnO samples, the absorption peaks slightly shifted to 301 and 292 nm. These peak shifted to the lower wavelength region (blue shift). This blue shift occurred due to quantum confinement effect [43] that led to the increase of the band gap energy and decrease in crystallite size [44]. Therefore, the optical property of ZnO thin film was strongly associated to the structural and morphological properties.

According to Viezbicke et al. [45] investigations, the optical absorption strength correlated to the difference between the photon energy and the band gap energy.

The optical absorption coefficient,  $\alpha$ , can be obtained from transmittance T, and thickness t, by following equation [46]:

$$\alpha = \ln (1/T)/t \tag{4}$$

The optical band gap (E<sub>g</sub>) of direct transition semiconductor was calculated by the expression:

$$(\alpha h\nu) = A (h\nu - E_g)^n \tag{5}$$

where E<sub>g</sub> is the optical band gap,  $\alpha$  is the

absorption coefficient, h is the Planck's constant,  $\nu$  is the incident light frequency and A is a constant that depends on the electron-hole mobility. The index n categorizes the type of electronic transition between the energy bands; the values of 1/2 and 2 are associated with direct and indirect transitions, respectively. The value of n is 1/2 for direct allowed transitions, which is the case of ZnO [47].

The optical band gap of the thin films can be examined by extrapolating the straight linear portion of the plots of  $(\alpha h\nu)^2$  versus the photon energy (h $\nu$ ) to the phonon energy axis, which is shown in the interior of Fig.7.

Using this method the optical band gap value obtained for ZnO nanoparticles was 3.91, 4.17 and 4.41 eV for 5%, 10% and 15% O<sub>2</sub> in plasma which are greater than that of bulk. The properties of particles with nano meter sized exhibit quite different from bulk materials because of some emergence

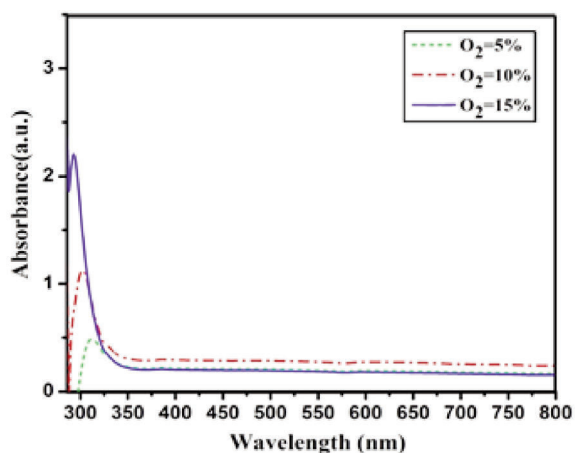


Figure 6. Optical absorbance spectra per wavelength

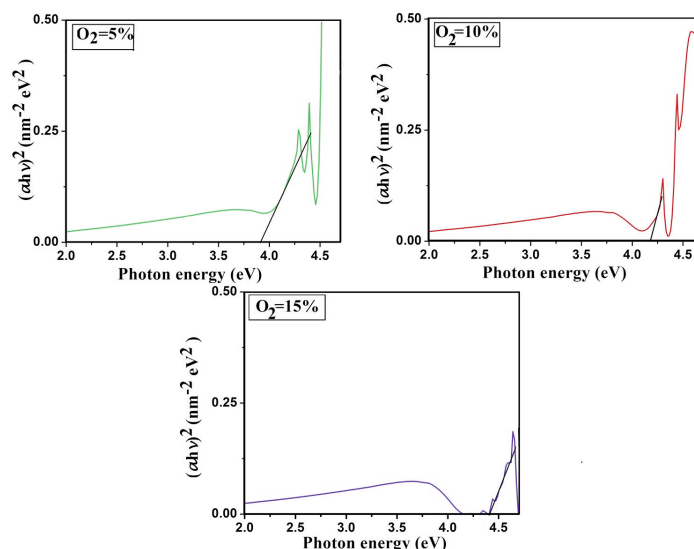


Figure 7. Optical band gap per photon energy



phenomenon like quantum size confinement, wave like transport and predominance of interfacial [48].

These results suggest that the O<sub>2</sub>/Ar ratios have a strong influence on absorption coefficient and absorption edge.

With increasing O<sub>2</sub> concentration in the plasma, the optical band gap increased. It reveals strong influence of optical band gap on O<sub>2</sub>/Ar ratios in the carrier gas. This phenomenon can be related to the decrease of the growth rates. However, the optical band gap of ZnO was affected by O<sub>2</sub> vacancies and Zn interstitial atoms, as well as the grain size [49]. The increased band gap in the blue shift part may be attributed to the change in the energy band gap of orbital's hybridization [50].

Moreover, the band gap increasing and decreasing of grain size can be explained with the Burstein–Moss effect [51]. The band widening effect is attributed to the increase in the fermi level of the conduction band [52].

#### 4. Conclusions

ZnO thin films were prepared on different substrates by DC reactive magnetron sputtering with 99.99% pure Zn metallic in different mixes of O<sub>2</sub>+ Ar as carrier gases. In the present work, the impact of different O<sub>2</sub> concentrations in carrier gas (5, 10 and 15%) on physical properties (structural, morphological and optical) of ZnO thin films was investigated and discussed. The different texture and micro-structural features of thin films were detected. The optimum growth conditions were found to be a compromise between crystalline quality and surface morphology. The XRD spectrums showed the hexagonal structures for all thin films. At lower O<sub>2</sub> concentration in plasma, well-textured h-ZnO nano crystallites with columnar grains were formed and the crystal quality of the films had slightly declined with the increase of O<sub>2</sub> concentration in plasma. All films had (101) peak at 37°. The presence of (101) crystal plane was less distinct with the increase of O<sub>2</sub> concentration in plasma. The increase of O<sub>2</sub> concentration in the gas mixture led to decrease in the (101) peak intensity and a little shifts to lower angles. According to the XRD data, the calculated strain showed that the strain for (101) plane orientation increased first and then decreased when the O<sub>2</sub> concentration increased. Surface topographies considered by AFM imaging showed that average roughness and grain sizes increased first and then decreased with the O<sub>2</sub> concentration increment. The increase in particle size of ZnO films and reduction of lattice strain were observed at 10% O<sub>2</sub>. The FE-SEM images showed some needle like grains dispersed over the substrate surface at lower O<sub>2</sub> concentration that transformed to irregular plate shaped grains at

10% O<sub>2</sub>. The increase of the O<sub>2</sub> concentration resulted in large grain size that occurred due to agglomeration. The variation in band gap directly showed the impact of O<sub>2</sub> concentration in gas mixture on optical properties. The optical band gaps were found to be size dependent and the band gap decreased with the particle size. A remarkable blue shift in optical band gap was observed with the increase of O<sub>2</sub> concentration and optical band gap value increase. The optical band gap of ZnO thin films was larger than the ZnO bulk (E<sub>g</sub> = 3.37 eV). The results show that O<sub>2</sub> concentration in carrier gas had an effective influence on the structural and optical properties of ZnO thin films.

#### Acknowledgments

*Authors are thankful to Department of physic of plasma physic center. This study was not funded. The authors declare that they have no conflict of interest.*

#### Reference

- [1] M. Ramani, S. Ponnusamy, C. Muthamizhchelvan, J. Cullen, S. Krishnamurthy, E. Marsili, Colloid. Surf. B: Biointerfaces, 105(2013) 24-40.
- [2] D.C. Look, B. Clafin, Ya.I. Alivov, S.J. Park, Phys. Status Solidi A, 201(10) (2004) 2203-2212.
- [3] A. Ashrafi, C. Jagadish, J. Appl. Phys., 102 (7) (2007) 071101.
- [4] R. Shabannia, J. Mol. Struct., 1118 (2016)157-160.
- [5] Ü. Özgür, Y.I. Alivov, C. Liu, A. Teke, M.A. Reshchikov, S. Doğan, V. Avrutin, S.J. Cho, H. Morkoç, J. Appl. Phys., 98 (4) (2005) 1.
- [6] Z.K. Tang, G.K.L. Wong, P. Yu, Appl. Phys. Lett., 72(25) (1998) 3270-3272.
- [7] J. Han, F. Fan, C. Xu, S. Lin, M. Wei, X. Duan, Zl. Wang, Nanotechnology, 21(2010) 405203-405210.
- [8] R.P. Yadav, D.C. Agarwal, M. Kumar, P. Rajput, D.S. Tomar, S.N. Pandey, P.K. Priya, A.K. Mittal, Appl. Surf. Sci., 415 (2017) 51-58.
- [9] T. S. Phely-Bobin, R. J. Muisener, J. T. Koberstein, F. Papadinmitrakopoulos, Synth. Met., 116 (2001) 439-443.
- [10] Zh. Zang, X. Tang, J. Alloy Compd., 619 (2015). 98-101.
- [11] F.H. Leiter, H.R. Alves, A. Hofstaetter, D.M. Hofmann, B.K. Meyer, Phys. Status Solidi B 226(1) (2001) R4-R5.
- [12] H.J. Egelhaaf, D. Oelkrug, J. Cryst. Growth 161(1996) 190-194.
- [13] L.S. Vlasenko, G.D. Watkins, Phys. Rev. B 72 (2005) 035203-035215.
- [14] G.T. Dang, T. Kawaharamura, N. Nitta, T. Hirao, T. Yoshiie, M. Taniwaki, J. Appl.Phys. 109(12) (2011) 123516-123521.
- [15] M.D. McCluskey, S.J. Jokela, J. Appl. Phys. 106 (2009) 71101.
- [16] S. Sadjadi, M. Eskandari, Ultra. Sonochem. 20(2) (2013) 640-643.



- [17] P. Yang, H. Yan, S. Mao, R. Russo, J. Johnson, R. Saykally, N. Morris, J. Pham, R. He, J.H. Choi, *Adv. Funct. Mater.* 12(5) (2002) 323-331.
- [18] Y. Sun, D.J. Riley, M.N.R. Ashfold, *J. Phys. Chem. B* 110(31) (2006) 15186-15192.
- [19] Z. Zang, M. Wen, W. Chen, Y. Zeng, Z. Zu, X. Zeng, X. Tang, *Mater. Des.* 84 (2015) 418-421.
- [20] Z. Zang, X. Tang, *J. Alloy Compd.*, 619 (2015) 98-101.
- [21] V. Bhardwaj, R. Chowdhury, R. Jayaganthan, *4332(16)* (2016)31670-1.
- [22] I. Hadjoub, T. Touam, A. Chelouche, M. Atoui, J. Solard, M. Chakaroun, A. Fischer, A. Boudrioua, L. H. Peng, *Appl. Phys. A: Mater. Sci. Proc.*, 122 (2016) 78.
- [23] R. Serhane, S. Abdelli-Messaci, S. Lafane, H. Khales, W. Aouimeur, A. Hassein- Bey, T. Boutkedjirt, *Appl. Surf. Sci.*, 288 (2014) 572-578.
- [24] X. Li, Z. Hu, J. Liu, D. Li, X. Zhang, J. Chen, J. Fang, *Appl. Catal., B*,195(2016) 29-38.
- [25] S. Fairose, S. Ernest, S. Daniel, *Sens. Imaging*, 19(1) (2018) 1-18.
- [26] I. Safi, *Surf. Coat. Tech.*, 127 (2000)203-218.
- [27] C. Ziebert and S. Ulrich, *J. Vac. Sci. Tech. A*, 24 (2006) 554.
- [28] P. Taneja, R. Banerjee, P. Ayyub, and G. K. Dey, *Phys. Rev. B – Cond. Matt. Mat. Phys.*, 64(3) (2001) 033405.
- [29] B. Abdallah, A. Kader Jazmatia, R. Refaia, *Mate. Res.*, 20(3) (2017) 607-612.
- [30] B. Szyszka, M. Vergo, R. Bandorf, G. Bra, *Vacu.*, 84(2010) 1354-1359.
- [31] P.S. Ho, *Thin Solid Films* 96(4) (1982) 301-316.
- [32] L. Huaxiang, L. Ding, W. Deng, X. Wang, J. Long, Q. Li., *Adv. Che. Eng. Sci.*, 3(4) (2013) 236-241.
- [33] D. K. Hwang, K. P. Kim, D.H. Kim, *Thin Solid Films* 546 (2013) 18-21.
- [34] S.I. Boyadjiev, V. Georgieva, R. Yordanov, Z. Raicheva, I.M. Szilágyi, *Appl. Surf. Sci.* 387 (2016) 1230-1235.
- [35] A. Dhanalakshmic, A. Palanimurugan, B. Natarajan, *Carbo. Poly.*, 168(2017) 191-200.
- [36] J.A. Najim, J.M. Rozaiq, *Int. Lett. Chem. Phys. Astron.* 10 (2) (2013)137.
- [37] J.E. Kelsey, C. Goldberg, G. Nuesca, G. Peterson, A. Kaloyeros, B. Arkles, *J. Vac. Sci. Technol. B* 17 (1999) 1101-1104.
- [38] A.R. Stokes, A.J.C. Wilson, *Proc. Phys. Soc.* 56 (1944) 174-181.
- [39] A. Purohit, S. Chander, A. Nehra, S.P. Nehra, C. Lal, M.S. Dhaka, *Physica E* 69 (2015) 342-348.
- [40] S.R. Bhattacharyya, A.K. Pal, *Ind. J. Pu. Appl. phys.*, 47 (2009)125-133.
- [41] M. Kwoka, B. Lyson-Sypien, A. Kulis, M. Maslyk, M. Adam Borysiewicz, E. Kaminska, J. Szuber, *mat.*, 11(1) (2013) 131.
- [42] J.A. Thornton, *J. Vac. Sci. Technol.* 11 (1974) 666-670.
- [43] A. Kalita, S. Karmakar, *Int. J. Sci. Res.*, 6(6) (2018) 122-126.
- [44] P.K. Samanta, A.K. Bhunia, T. Kamilya, *J. Nano. Elec. Phys.*, 6(2) (2006)1-2.
- [45] B.D. Viezbicke, S. Patel, B.E. Davis, D.P. Birnie III, *Phys. Status Solidi B* 8 (2015)1700-1710.
- [46] C. Lung, M. Toma, M. Pop, D. Marconi, A. Pop, *J. Alloy Compd.*, 725 (2017) 1238-1243.
- [47] P. Kalita, B. Sharma, *Bull. Mat. Sci.* 23(4) (2000) 313-317.
- [48] H. Sarma, D. Chakraborty, K.C. Sarma, *Int. J. Inno. Res. Sci. Engineering and Technology*, 3 (2014)16957-16964.
- [49] M. Suche, S. Christoulakis, N. Katsarakis, T. Kitsopoulos, G. Kiriakidis, *Thin Solid Films*, 515(16) (2007) 6562-6566.
- [50] Y. Zhang, H. Jia, P. Li, F. Yang, Z. Zheng, *Opt. Comm.*, 284 (2011)236-239.
- [51] P. Prathap, N. Revathi, Y.P.V. Subbaiah, K.T.R. Reddy, *J. Phys.: Condens. Matter.* 20(3) (2007) 035205.
- [52] Q.B. Ma, Z.Z. Ye, H.P. He, S.H. Hu, J.R. Wang, L.P. Zhu, Y.Z. Zhang, B.H. Zhao, *J. Crys. Growth* 304 (2007)64-68.



## FIZIČKE OSOBINE TANKOG SLOJA ZnO SA NANO STRUKTUROM KOJI JE NANET METODOM DC MAGNETRONSKOG RASPRŠIVANJA U PRISUSTVU RAZLIČITIH KONCENTRACIJA O<sub>2</sub> U NOSEĆEM GASU

S. Asgary <sup>a</sup>, A.H. Ramezani <sup>a</sup>, A. Mahmoodi <sup>b</sup>

<sup>a</sup> Odsek za fiziku, Ogranak u zapadnom Teheranu, Islamski slobodni univerzitet, Teheran, Iran

<sup>b</sup> Centar za istraživanje plazme, Ogranak za nauku i istraživanje, Islamski slobodni univerzitet, Teheran, Iran

### Apstrakt

Tanki slojevi ZnO visokog kvaliteta sa polikristalnom heksagonalnom strukturom (101) orijentacije su naneti na Si i granulisanu staklenu podlogu putem metode reaktivnog magnetronskog raspršivanja jednosmernom strujom. Ispitivan je uticaj različitih koncentracija kiseonika u nosećem gasu na strukturne, morfološke i optičke osobine. Povećanje koncentracije O<sub>2</sub> je dovelo do smanjenja inteziteta glavne orijentacije i pomeranja najviše vrednosti na niže 2θ vrednosti. Na slikama dobijenim skenirajućim elektronskim mikroskopom se može videti porozna struktura u obliku stuba koja se sužava koja je slična zoni 1 Torntonove strukturne zone modela kada je sadržaj O<sub>2</sub> najviši. Na AFM slikama se može videti morfologija tankog sloja, kao i hrapavost površine na koje uticala koncentracija O<sub>2</sub>. UV-Vis-NIR merenja su pokazala da je intezitet apsorpcije UV zraka kod uzoraka povećan i da je pomeren na kraće talasne dužine (plava svetlost) kada je koncentracija O<sub>2</sub> bila viša. Povrh toga, optička zabranjena zona se povećala sa 3,91 na 4,41 eV kao funkcija koncentracije kiseonika.

**Ključne reči:** DC magnetronsko raspršivanje; Porozni tanki sloj ZnO; Strukturne osobine; Morfološke osobine; Optička zabranjena zona; Apsorpcija.

